Comparison of Different Period Digital Alloy $Al_{0.7}InAsSb$ Avalanche Photodiodes

Yuan Yuan, Ann K. Rockwell, Yiwei Peng, Jiyuan Zheng, Stephen D. March, Andrew H. Jones, Min Ren, Seth R. Bank, and Joe C. Campbell, *Fellow, IEEE*

***Abstract* — We report $Al_{0.7}InAsSb$ avalanche photodiodes grow as ternary-binary and binary-binary digital alloys. Their characteristics of ideality factor, activation energy, temperature-dependent excess noise, temperature stability, and impact ionization coefficients are compared.**

***Index Terms*—Avalanche breakdown, low noise, photodiodes, III-V semiconductor materials.**

I. Introduction

Owing to their internal gain, avalanche photodiodes (APDs) have been widely used in long-haul telecommunications, LIDAR, data centers, military and research applications where high receiver sensitivity is vital. However, the gain of APDs varies from one injected carrier to the next because impact ionization is a random process. This is a source of noise that is typically expressed as the excess noise factor, $F\langle M\rangle$, which is incorporated as a multiplicative factor in the shot noise, which becomes [1,2]:

$$\left\langle i_{shot}^2 \right\rangle = 2q\left(I_{photo}+I_{dark}\right)\left\langle M\right\rangle^2 F\left\langle M\right\rangle \Delta f\,, \tag{1}$$

where I_{photo} is photocurrent, I_{dark} is dark current, $\langle M\rangle$ is average gain, and Δf is bandwidth. In the local field model the excess noise factor is given by the following expression [3]:

$$F\left\langle M\right\rangle = kM + (1-k)(2-1/M)\,, \tag{2}$$

where k is the ratio of the hole ionization coefficient, β, to that of the electron, α, i.e. $k=\beta/\alpha$. It is clear that the excess noise factor increases with gain but increases more slowly for low values of k, i.e., for fixed gain, low k results in lower excess noise. The tradeoff between the benefit of avalanche gain and the gain-linked noise is revealed in the signal to noise ratio (SNR),

$$SNR = \frac{I_{photo}^2}{2qI_{total}F\left\langle M\right\rangle \Delta f + \dfrac{\sigma_{circuit}^2}{M^2}}, \tag{3}$$

where $\sigma_{circuit}^2$ is the root mean square noise current of the following electronic circuit. In effect, the multiplication gain of the APD suppresses the circuit noise until the APD noise is comparable to that of the circuit. Thus, low excess noise, i.e. low k-value, is beneficial in that it permits higher gain values and consequently higher receiver sensitivity.

Recently, we have demonstrated APDs with $Al_xIn_{1-x}As_ySb_{1-y}$ digital alloy multiplication regions on GaSb substrate [4-8] and $In_{0.52}Al_{0.48}As$ digital alloy grown on InP [9,10]. These III-V digital alloy APDs exhibit similar low excess noise to Si APDs, while they have direct bandgap, high absorption coefficients, wider spectral response region and flexible complex structure design. In this work we report APDs fabricated from two types of $Al_xIn_{1-x}As_ySb_{1-y}$ digital alloys with 70% Al concentration. In one, the fundamental period of the digital alloy consists of the binaries InAs, InSb, AlSb, and AlAs [11-13], referred to in the following as the binary digital alloy. The other is comprised of InAs, InSb, and the ternary $AlAs_{0.1}Sb_{0.9}$, which will be denoted as the ternary digital alloy (even though it contains two binaries). A primary motivation for comparing the binary and ternary digital alloys is that the ternary digital alloy has reduced valence band offsets [14], which may reduce the miniband in the valence. This can affect hole transport [15]. In this paper we report that both digital alloy p-i-n APDs exhibit low noise and excellent temperature stability. We also compare their ideality factors, activation energies, temperature-dependence of excess noise, variation of breakdown with temperature, and the ionization coefficients, α and β, of $Al_xIn_{1-x}As_ySb_{1-y}$ digital alloys.

II. Device Structure and Fabrication

The binary and ternary digital alloys were grown on GaSb and InAs substrates, respectively. The period thicknesses of these two $Al_{0.7}InAsSb$ digital alloys are both 10 monolayers (ML), and the fundamental periods are shown in Fig. 1.

This article has been accepted for publication in a future issue of this journal, but has not been fully edited. Content may change prior to final publication. Citation information: DOI 10.1109/JLT.2019.2918676, Journal of Lightwave Technology

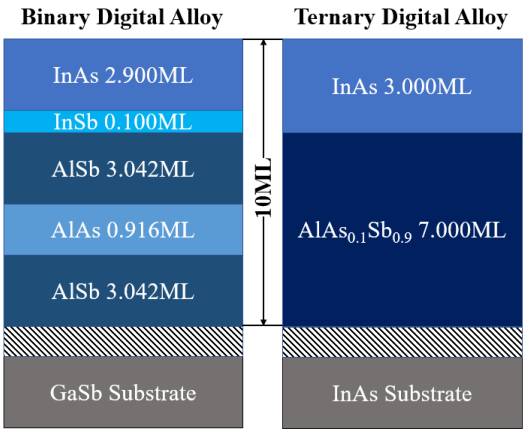

Figure 1. Period information of two $Al_{0.7}InAsSb$ digital alloys.

APDs with p-i-n and n-i-p structures with the same multiplication region thickness were grown in so as to determine the ionization coefficients through measurements with pure electron and pure hole injection method. The layer structures are shown in Table I. Be and Te were used as p-type and n-type layers doping, respectively.

TABLE I
STRUCTURES OF DIGITAL ALLOY APDS

Types	Material	Doping (cm^{-3})	Thickness(nm)
Binary Digital Alloy p-i-n APD	GaSb	p: 1×10^{19}	100
	$Al_{0.7}InAsSb$	p: 2×10^{18}	100
	$Al_{0.7}InAsSb$	UID	1000
	$Al_{0.7}InAsSb$	n: 2×10^{18}	200
	GaSb	n: 2×10^{18}	300
	GaSb	n: 1×10^{17}	substrate
Binary Digital Alloy n-i-p APD	GaSb	n: 1×10^{19}	100
	$Al_{0.7}InAsSb$	n: 2×10^{18}	100
	$Al_{0.7}InAsSb$	UID	1000
	$Al_{0.7}InAsSb$	p: 2×10^{18}	200
	GaSb	p: 2×10^{18}	300
	GaSb	p: 1×10^{17}	substrate
Ternary Digital Alloy p-i-n APD	InAs	p: 1×10^{19}	100
	$Al_{0.7}InAsSb$	p: 2×10^{18}	100
	$Al_{0.7}InAsSb$	UID	1000
	$Al_{0.7}InAsSb$	n: 2×10^{18}	200
	InAs	n: 2×10^{18}	300
	InAs	n: 1×10^{17}	substrate
Ternary Digital Alloy n-i-p APD	InAs	n: 1×10^{19}	100
	$Al_{0.7}InAsSb$	n: 2×10^{18}	100
	$Al_{0.7}InAsSb$	UID	1000
	$Al_{0.7}InAsSb$	p: 2×10^{18}	200
	InAs	p: 2×10^{18}	300
	InAs	p: 1×10^{17}	substrate

All four mesa types were formed by a combination of dry etching and wet etching to reduce surface dark current. The mesas were dry etched ~ 1μm using reactive ion etching (RIE) and inductively coupled plasma (ICP). This was followed with a wet etch in critic acid solution. Top and bottom contacts were deposited with Ti and Au by electron-beam evaporation. Finally, the sidewall was passivated by spinning SU8 to further reduce surface dark current.

III. DEVICE CHARACTERISTICS

A. Multiplication Gain and Capacitances

In this letter, all measurements were carried out with 100 μm-diameter APDs. Figure 2 shows the total current, dark current, and multiplication gain versus bias voltage for the four types of APDs. All were illuminated with a 543 nm He-Ne CW laser. The blue dash lines denote pure electron injection gain, M_e, and the red dash lines represent pure hole injection gain, M_h. The gain curves indicate that $\alpha > \beta$ in both the binary and ternary digital alloys since $M_e > M_h$.

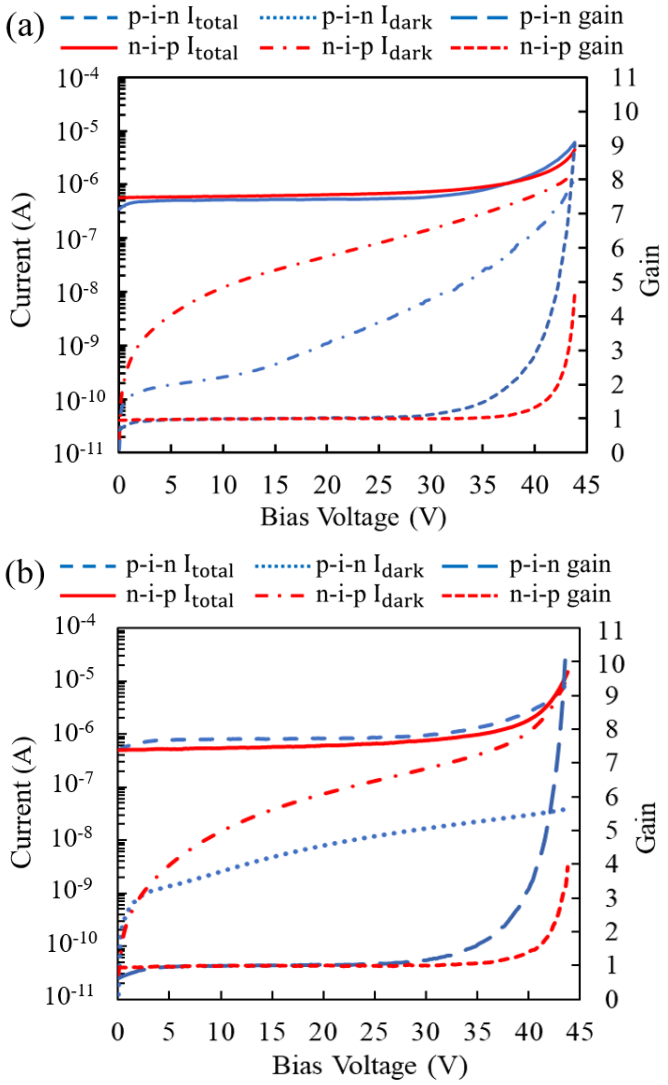

Figure 2. Total current, dark current, and gain versus bias voltage for (a) binary digital alloy p-i-n and n-i-p APDs, and (b) ternary digital alloy p-i-n and n-i-p APDs.

The gain characteristics of APDs vary with the depletion width. Capacitance-voltage measurements were carried out to ensure the depletion region thicknesses of the p-i-n and n-i-p APDs are same. In Fig. 3, the capacitances for these APDs are all ~ 0.8 pF when fully depleted, which means that the electric fields are comparable for the same voltages.

This article has been accepted for publication in a future issue of this journal, but has not been fully edited. Content may change prior to final publication. Citation information: DOI 10.1109/JLT.2019.2918676, Journal of Lightwave Technology

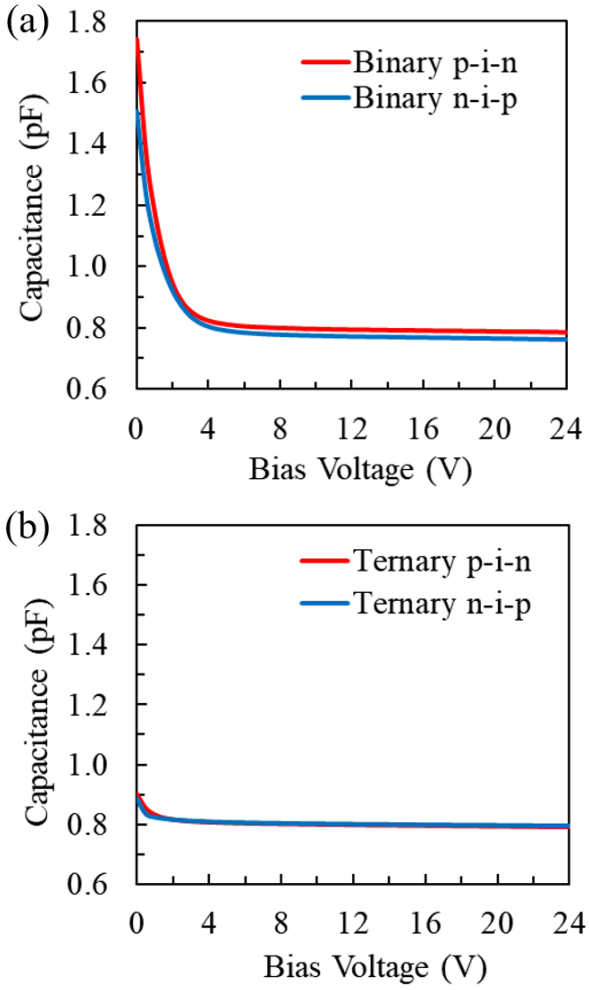

Figure 3. Capacitance voltage measurements for (a) binary and (b) ternary digital alloy APDs.

B. *Ideality Factors*

The forward current-voltage characteristics for p-i-n APDs from 213 K to 313 K are represented in Fig. 4 (a) and (b). The ideality factor, *n,* at different temperatures can be fitted using Eq. 4 below [16]

$$J_f \propto \exp\left(\frac{qV}{nk_BT}\right)-1, \tag{4}$$

where J_f is the forward current density, k_B is the Boltzmann constant, and T is the absolute temperature. The fitted dashed lines agree well with the experimental results, and the ideality factors of the binary and ternary diodes are plotted in Fig. 4 (c).

The forward current density of a p-i-n photodiode can be represented as [17]

$$J_f = J_d(e^{qV/k_BT}-1)+J_{nr}(e^{qV/2k_BT}-1)+J_r(e^{qV/k_BT}-1), \tag{5}$$

where the first item J_d is the diffusion component current density which ideality factor n = 1, the second item J_{nr} represents the Schottky-Read-Hall recombination component current density with n = 2, and the last item J_r is the radiative recombination component current density with n = 1. From Fig. 4 (c), we see that in the ternary material, the Schottky-Read-Hall recombination current density dominates, which illustrates that the ternary material has higher trap density. Also, the ideality factors decrease with increasing temperature.

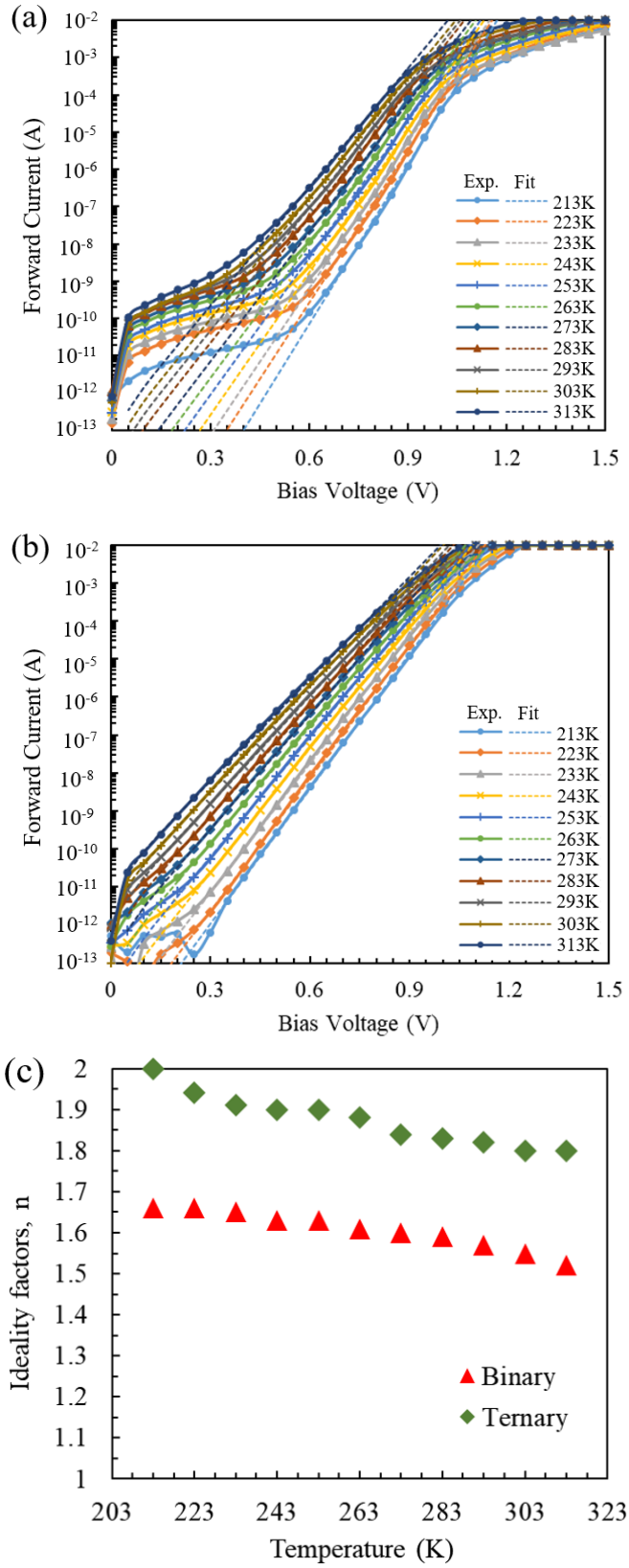

This article has been accepted for publication in a future issue of this journal, but has not been fully edited. Content may change prior to final publication. Citation information: DOI 10.1109/JLT.2019.2918676, Journal of Lightwave Technology

Figure 4. Forward current-voltage characteristics at different temperatures for the (a) binary and (b) ternary digital alloy p-i-n APDs. (c) Ideality factors versus temperature.

C. *Activation Energy*

The temperature dependent dark current of APDs is proportional to the function below [18, 19]:

$$I_{dark} \propto T^2 \exp(\frac{-E_a}{k_B T}), \quad (6)$$

where E_a is the activation energy. Figure 5 shows the dark current fits using Eq. 6 at reverse bias 5V, 10V, and 15V. The activation energies for the binary and ternary digital alloys are 0.14 eV and 0.23 eV, respectively, at all three bias voltages. It appears that the dominant generation-recombination center of the ternary material is deeper than that of the binary material.

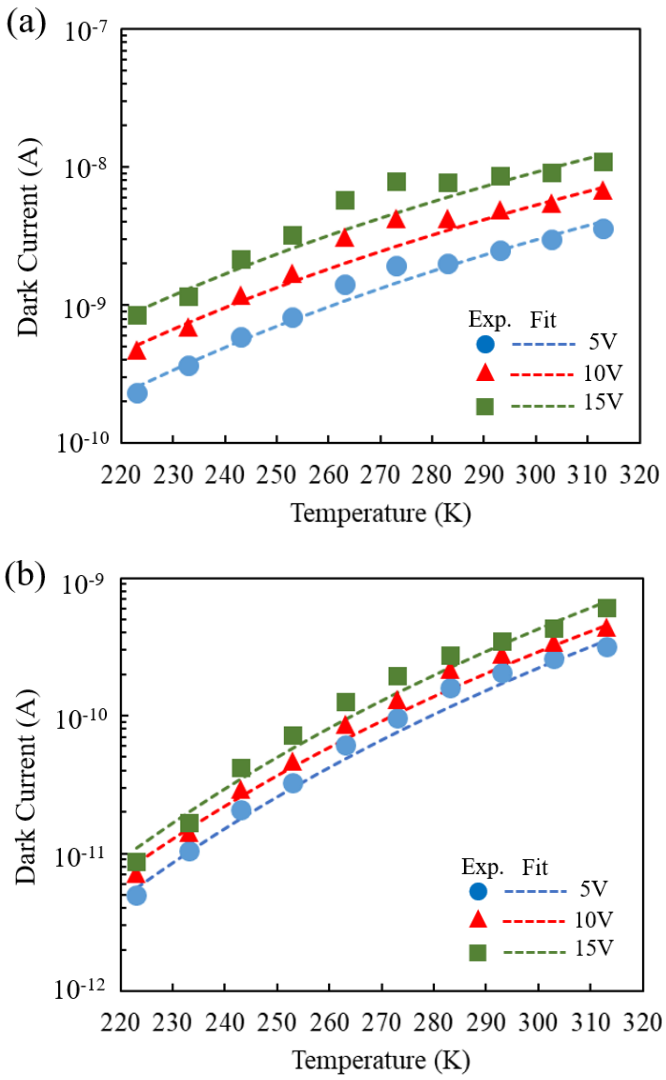

Figure 5. Dark current versus temperature for (a) binary and (b) ternary digital alloy p-i-n APD.

D. *Temperature-dependent Breakdown Voltage*

The temperature stability of APDs is an important figure of merit. In many applications, APDs are operated with a temperature controller to maintain constant multiplication gain. This is due to the fact that phonon scattering increases with temperature, which causes carriers to require higher electric field in order to impact ionize. The temperature stability of APDs can be evaulated by the breakdown voltage temperature coefficient $\Delta V_{bd}/\Delta T$. For the purpose of diminishing the complexity and cost of the temperature control system, a smaller $\Delta V_{bd}/\Delta T$ is desirable.

Recently, the digital alloy $Al_xInAsSb$ APDs have exhibited much smaller $\Delta V_{bd}/\Delta T$ than InP and random alloy InAlAs APDs [20, 21]. The breakdown voltages of these APDs were measured with a 543 nm He-Ne CW laser for pure electron injection. Fig. 6 (a) shows the breakdown voltage as a function of ambient temperature. The avalanche breakdown for the binary digital alloy occurs at lower electric field than that for the ternary. Recall that the depletion region thicknesses are the same for both types of APDs. From the slopes of the fitted functions, the $\Delta V_{bd}/\Delta T$ is 5.3 mV/K for the binary, and 3.9 mV/K for the ternary. Comparison of these two 1000 nm multiplication thickness digital alloy materials, one 890 nm binary $Al_{0.7}InAsSb$, one 890 nm binary $Al_{0.6}InAsSb$ and other conventional semiconductor materials are plotted in Fig. 6 (b). The temperature stability of the digital alloys is comparable to 100 nm thick AlGaAsSb and significantly lower than InP, InAlAs, and Si [24].

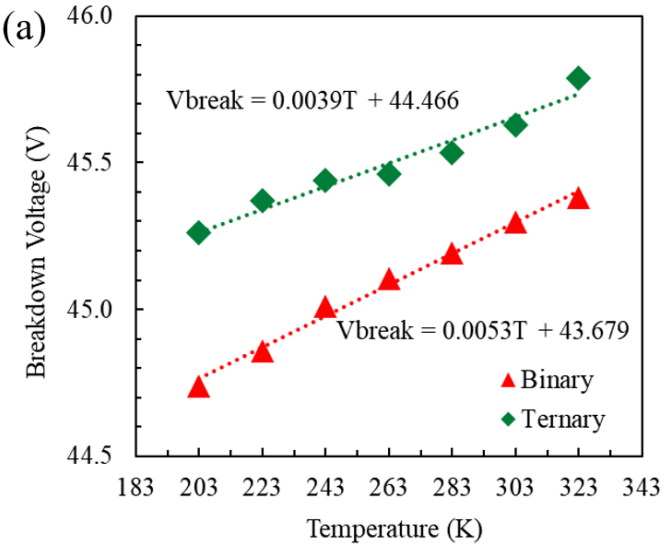

This article has been accepted for publication in a future issue of this journal, but has not been fully edited. Content may change prior to final publication. Citation information: DOI 10.1109/JLT.2019.2918676, Journal of Lightwave Technology

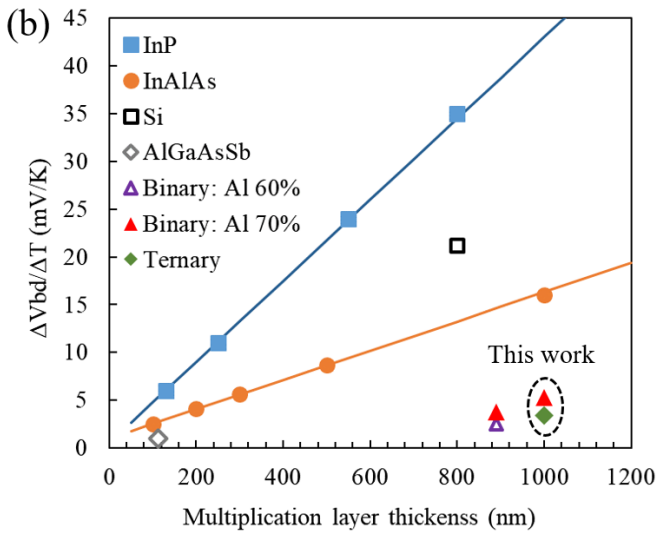

Figure 6. (a) Breakdown voltages versus temperature for both $Al_{0.7}InAsSb$ p-i-n APDs. (b) Temperature dependence of breakdown voltages for different materials [21-24].

E. Excess Noise

APDs fabricated from binary $Al_{0.7}InAsSb$ based on GaSb have exhibited very low excess noise with k values ~ 0.01, which is comparable to that of Si APDs [7]. The excess noise for the binary and ternary p-i-n APDs were measured with an HP 8970B noise figure meter and a 543 nm He-Ne CW laser. As shown in Fig. 7 (a), these two types of $Al_{0.7}InAsSb$ digital alloys exhibit the same excess noise characteristics. The excess noise factors for these two p-i-n APDs and AlGaAsSb [25, 26], AlAsSb [27], InP [28], InAlAs [29], Si [30] and InAlAs digital alloy [9] APDs at M= 10 are plotted in Fig. 7 (b). Typically, thin multiplication layers exhibit lower noise than bulk materials due to the non-local effect [31-33]. Compared to other APDs, these two materials achieve very low excess noise factors even with thick multiplication regions.

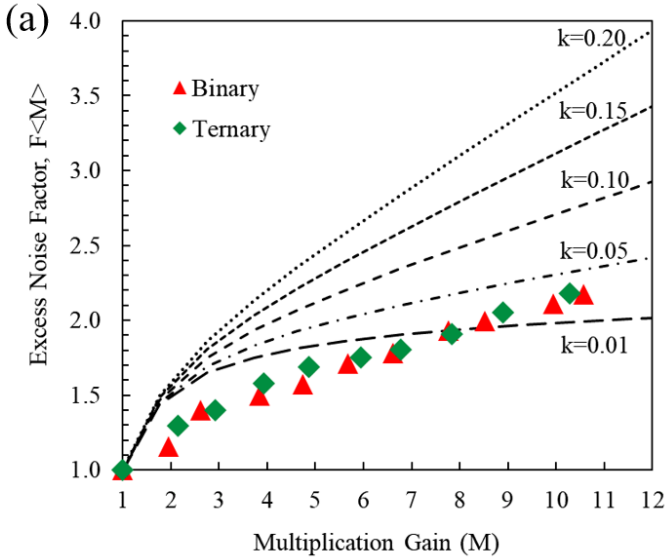

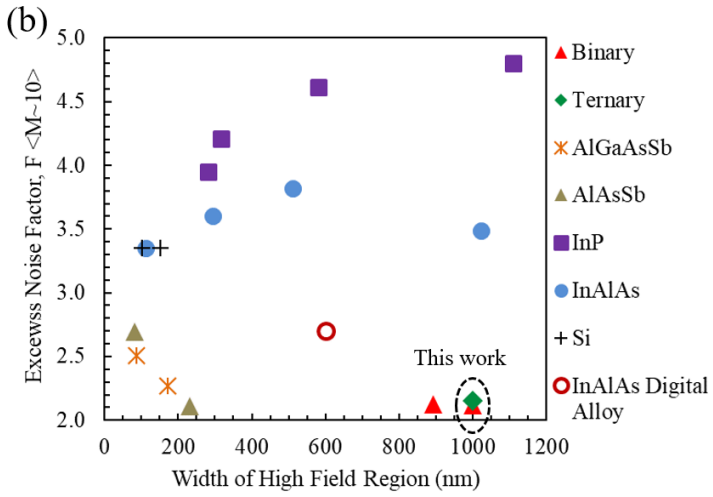

Figure 7. (a) Excess noise of binary and ternary digital alloy $Al_{0.7}InAsSb$ p-i-n APDs. (b) Comparison of excess noise factor at gain of 10 for different materials APDs [5], [9], [25-30].

Digital alloy InAlAs APDs have demonstrated lower excess noise than random alloy InAlAs APDs [9, 34]. The band structure of an $In_{0.52}Al_{0.48}As$ digital alloy has been simulated by using an environment-dependent tight binding model [35]. It was found that there are mini-gaps in the valence band, which could impede holes from initiating impact ionization [9,10]. To verify this hypothesis, the excess noise of the InAlAs digital alloy APDs was measured from 203 K to 323 K, and it was found that the k value decreases exponentially with decreasing temperature [9].

Similar results are observed for the digital alloy $Al_{0.7}InAsSb$ APDs studied here. Figures 8 (a) and 8 (b) show the temperature variation of excess noise for the binary and ternary APDs, respectively. Figure 8 (c) shows k versus temperature. Since the k value varies a little with the multiplication gain, the k values plotted are those for M = 11. Similar to the digital alloy InAlAs APDs, the k values also decrease exponentially with decreasing temperature for both the binary and ternary materials. The temperature dependences of the binary and ternary APDs can be expressed as Eq. 7 and 8, respectively:

$$k = 4.0\times10^{-5}\times\exp(0.0247\times T), \quad (7)$$

$$k = 1.5\times10^{-5}\times\exp(0.0247\times T). \quad (8)$$

This article has been accepted for publication in a future issue of this journal, but has not been fully edited. Content may change prior to final publication. Citation information: DOI 10.1109/JLT.2019.2918676, Journal of Lightwave Technology

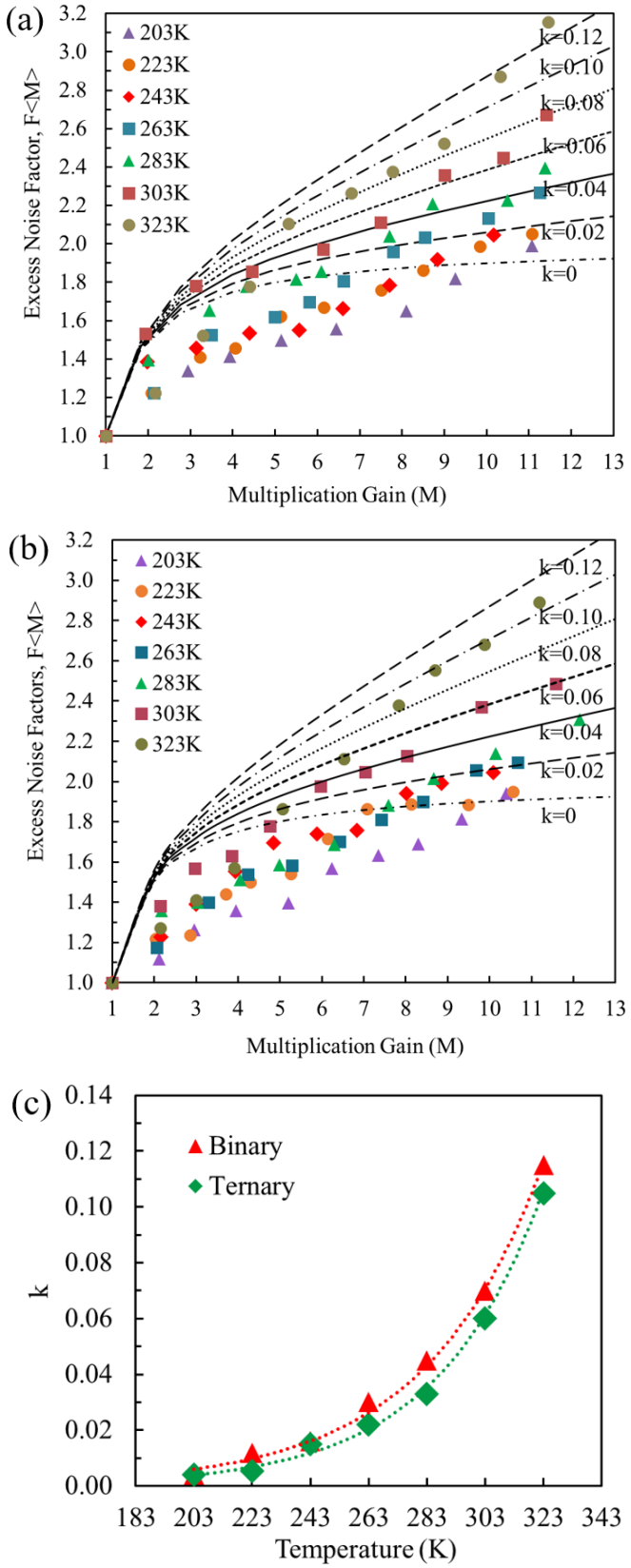

Figure 8. Temperature dependence of excess noise for (a) binary and (b) ternary digital alloy p-i-n APDs. (c) Ionization coefficient ratio *k* for binary and ternary digital alloy p-i-n APDs.

F. Impact Ionization

Figure 2 shows the multiplication gain curves for p-i-n and n-i-p APDs under pure electron or hole injection. The thicknesses of the depletion region, *W*, are the same for the p-i-n and n-i-p APDs. Using Eq. 9 and 10 below [36]

$$\alpha(E)=\frac{1}{W}\left[\frac{M_n(V)-1}{M_n(V)-M_p(V)}\right]\ln\left[\frac{M_n(V)}{M_p(V)}\right], \quad (9)$$

$$\beta(E)=\frac{1}{W}\left[\frac{M_p(V)-1}{M_p(V)-M_n(V)}\right]\ln\left[\frac{M_p(V)}{M_n(V)}\right], \quad (10)$$

the electric-field-dependent impact ionization coefficients for electrons (α) and holes (β) can be calculated. The calculations inculde the built-in voltage in order to obtain accurate electric field values. The built-in voltage is estimated with equtions as [37]

$$V_{bi}=\frac{k_BT}{q}\ln\left(\frac{N_dN_a}{n_i^2}\right), \quad (11)$$

$$n_i=\sqrt{N_CN_V}\exp\left(\frac{-E_g}{2k_BT}\right), \quad (12)$$

where both of these materials have same bandgap energy, E_g, of 1.13eV, and the values of N_C, N_V can be approximated with the parameters for $Ga_xInAsSb$ [38]: $N_C = 2.5\times10^{19}\times(0.022+0.03x-0.012x^2)^{3/2}$, $N_V = 2.5\times10^{19}\times(0.41+0.16x+0.23x^2)^{3/2}$, where $x=0.7$. Therefore,V_{bi} is around 1.14 V [39]. The calculated results for α and β are plotted as open points in Fig. 9. The measurements can be fit to the following expressions for the binary digital alloy:

$$\alpha(E)=3.5\times10^6\times\exp(-2.4\times10^6/E), \quad (13)$$

$$\beta(E)=1.0\times10^7\times\exp(-3.55\times10^6/E), \quad (14)$$

and

$$\alpha(E)=4.0\times10^6\times\exp(-2.5\times10^6/E), \quad (15)$$

$$\beta(E)=1.9\times10^8\times\exp(-4.8\times10^6/E), \quad (16)$$

for the ternary alloy. The fits are plotted as solid lines in the figures.

This article has been accepted for publication in a future issue of this journal, but has not been fully edited. Content may change prior to final publication. Citation information: DOI 10.1109/JLT.2019.2918676, Journal of Lightwave Technology

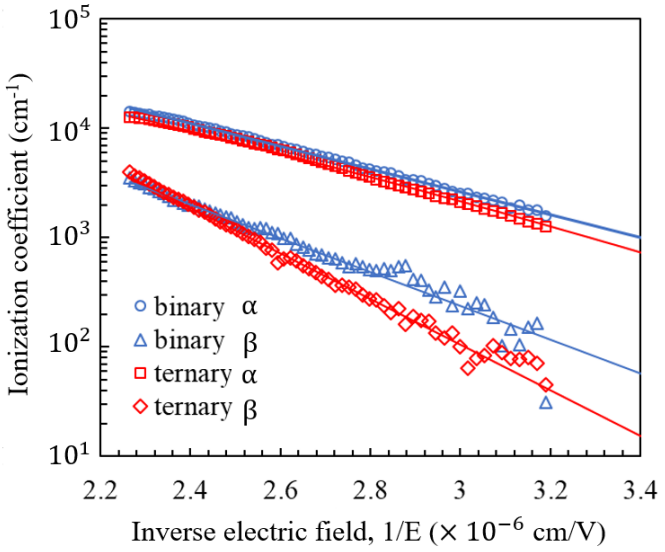

Figure 9. Ionization coefficients for $Al_{0.7}InAsSb$ binary and ternary digital alloy p-i-n APDs.

In Fig. 8 (c), the k value changes exponentially with temperature. These k values were used to calculate the temperature dependence of the ionization coefficients using the following expressions [9], [40]:

$$\alpha(E) = \frac{\ln\left[k-(k-1)/M_e(V)\right]}{(k-1)\times W}, \tag{17}$$

$$\beta(E) = k\times\alpha(E). \tag{18}$$

As shown in Fig. 10, for both the binary and ternary alloys, due to increased phonon scattering at higher temperature, the electron impact ionization coefficients display modest reduction with temperature. However, the hole impact ionization coefficients exhibit the significant change; β increases rapidly with temperature. It follows that the observed decrease in excess noise with decreasing temperature is primarily due to the reduction of the hole ionization coefficient.

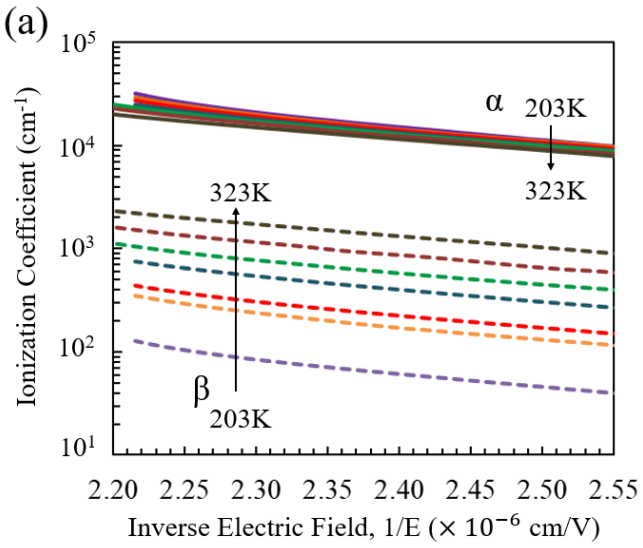

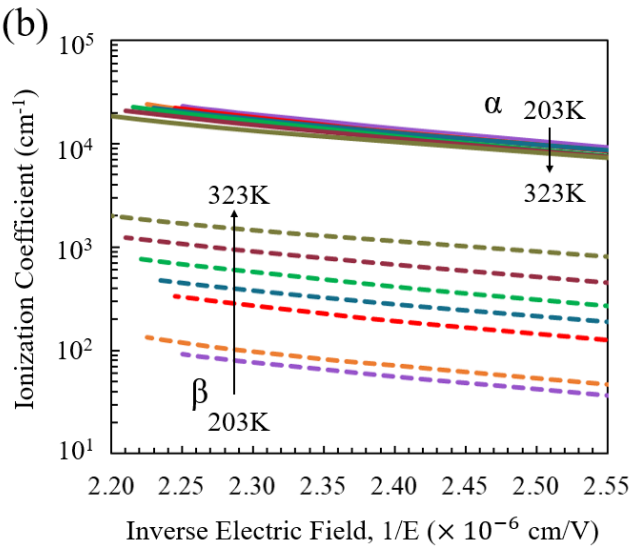

Figure 10. Temperature dependence of ionization coefficients for $Al_{0.7}InAsSb$ (a) binary and (b) ternary digital alloy p-i-n APD.

IV. Conclusion

In conclusion, digital alloy $Al_{0.7}InAsSb$ APDs having two different periods have been studied. Both exhibit very low excess noise and high thermal stability. The excess noise performance at different temperatures exhibits an exponential relation with temperature. The impact ionization coefficients for these two types $Al_{0.7}InAsSb$ APDs have been measured and it was found that the hole ionization coefficient exhibits significant reduction at lower temperature, while that of the electron is relatively independent of temperature.

References

[1] R. J. McIntyre, "Multiplication noise in uniform avalanche photodiodes" *IEEE Trans. Electron Dev*. ED-13, 64 (1966).

[2] J. C. Campbell, "Recent Advances in Avalanche Photodiodes," *J. Lightwave Tech.,* 34(2), 278-285 (2016).

[3] J. C. Campbell, "Advances in photodetectors," in *Optical Fiber Telecommunications, Part A: Components and Subsystems*, 5th ed., edited by I. Kaminow, T. Li, and A. E. Wilner (Academic Press, 2008), Vol. 5.

[4] Seth R. Bank, et al. "Avalanche Photodiodes Based on the AlInAsSb Materials System." *IEEE J. Sel. Top. Quantum Electron.,* 24.2 (2018): 1-7.

[5] M. Ren, et al. "Characteristics of $Al_xIn_{1-x}As_ySb_{1-y}$ (x: 0.3−0.7) Avalanche Photodiodes." *J. Lightwave Tech.,* 35.12 (2017): 2380-2384.

[6] M. Ren, et al. "AlInAsSb separate absorption, charge, and multiplication avalanche photodiodes." *Appl. Phys. Lett.,* 108.19 (2016): 191108.

[7] M. E. Woodson, et al. "Low-noise AlInAsSb avalanche photodiode. " *Appl. Phys. Lett.,* 108.8 (2016): 081102.

[8] A. K. Rockwell, et al. "Al 0.8 In 0.2 As 0.23 Sb 0.77 Avalanche Photodiodes." *IEEE Photo. Tech. Lett.,* 30.11 (2018): 1048-1051.

[9] Y. Yuan, et al. "Temperature dependence of the ionization coefficients of InAlAs and AlGaAs digital alloys." *Photo. Research,* 6.8 (2018): 794-799.

[10] J. Zheng, et al. "Digital Alloy InAlAs Avalanche Photodiodes." *J. Lightwave Tech.* (2018).

[11] S. J. Maddox, et al. "Broadly tunable AlInAsSb digital alloys grown on GaSb." *Crystal Growth & Design* 16.7 (2016): 3582-3586.

[12] L. G. Vaughn, *et al*. "Type I mid-infrared MQW lasers using AlInAsSb barriers and InAsSb wells," *Proc. SPIE*, vol. 5722, pp. 307–318, Apr. 2005.

[13] L. G. Vaughn, *et al*. "Characterization of AlInAsSb and AlGaInAsSb MBE-grown digital alloys," in *Proc. Mat. Res. Soc. Symp*., vol. 744. Jan. 2003, pp. M7.2.1–M7.2.12.

[14] A. K. Rockwell, et al. "Toward Deterministic Construction of Low Noise Avalanche Photodetector Materials," *Appl. Phys. Lett.*, (2018).

[15] I. Vurgraftman, et al. "Band parameters for III-V compound semiconductors and their alloys," *J. of Appl. Phys*. 89, 5815 (2001).

[16] D. M. Kim, et al. "Characterization and modeling of temperature-dependent barrier heights and ideality factors in GaAs Schottky diodes." *Solid-state electronics* 51.6 (2007): 865-869.

[17] Z. Hu, et al. "Near unity ideality factor and Shockley-Read-Hall lifetime in GaN-on-GaN pn diodes with avalanche breakdown." *Appl. Phys. Lett.* 107.24 (2015): 243501.

[18] W. Sun *et al*. "High-gain InAs avalanche photodiodes," *IEEE J. Quantum Electron*., vol. 49, no. 2, pp. 154–161, Feb. 2013.

[19] K. Sun, et al. "Pulse laser sulfur-hyperdoping of germanium and high quantum efficiency photodiodes." *IEEE Photon. J.* 8.5 (2016): 1-10.

[20] M. Ren, et al. "Operation stability study of AlInAsSb avalanche photodiodes." *Photonics Conference (IPC),* IEEE, 2017.

[21] A. H. Jones, et al. "Al x In 1-x As y Sb 1-y photodiodes with low avalanche breakdown temperature dependence." *Optics Exp*. 25.20 (2017): 24340-24345.

[22] L. J. J. Tan, et al. "Temperature Dependence of Avalanche Breakdown in InP and InAlAs," *IEEE J. Quantum Electron.* 46(8), 1153–1157 (2010).

[23] D. J. Massey, et al. "Temperature Dependence of Impact Ionization in Submicrometer Silicon Devices," *IEEE Trans. Electron Dev.* 53(9), 2328–2334 (2006).

[24] X. Zhou, et al. "Thin Al_{1-x} Ga $_x$ $As_{0.56}Sb_{0.44}$ Diodes with Extremely Weak Temperature Dependence of Avalanche Breakdown," *R. Soc. Open Sci.* 4(5), 170071 (2017).

[25] L. L. G. Pinel, et al. "Effects of carrier injection profile on low noise thin Al0.85Ga0.15As0.56Sb0.44 avalanche photodiodes." *Optics exp*. 26.3 (2018): 3568-3576.

[26] X. Zhou, et al. "Thin Al1-xGaxAs0.56Sb0.44 Diodes With Low Excess Noise," *IEEE J. Sel. Top. Quantum Electron.* 24(2), 3800105 (2018).

[27] J. Xie, et al. "Excess Noise Characteristics of Thin AlAsSb APDs," *IEEE Trans. Electron Dev.* 59(5), 1475–1479 (2012).

[28] P. Yuan, et al. "Impact Ionization Characteristics of III-V Semiconductors for a Wide Range of Multiplication Region Thicknesses," *IEEE J. Quantum Electron*. 36(2), 198–204 (2000).

[29] Y. L. Goh, et al. "Excess Avalanche Noise in In0.52Al0.48As," *IEEE J. Quantum Electron.* 43(6), 503– 507 (2007).

[30] C. H. Tan, et al. "Avalanche Noise Measurement in Thin Si p+ -i-n+ Diodes," Appl. Phys. Lett. 76(26), 3926–3928 (2000).

[31] G. J. Rees, et al. "Nonlocal impact ionization and avalanche multiplication," *J. Phys. D: Appl. Phys*., 43, 243001 (2010).

[32] M. M. Hayat, et al. "Effect of dead space on gain and noise of double-carrier-multiplication avalanche photodiodes," *IEEE Trans. Electron Dev*., vol. 39, no. 3, pp. 546–552, Mar. 1992.

[33] X. W. Li, et al. "Calculation of gain and noise with dead space for GaAs and AlxGa1-xAs avalanche photodiode," *IEEE Trans. Electron Dev*., vol. 49, no. 7, pp. 1112–1117, Jul. 2002.

[34] J. C. Campbell, et al. "Low-noise, infrared digital-alloy avalanche photodiodes." *Image Sensing Tech.: Mater., Dev., Syst., and Appl. V*. Vol. 10656. International Society for Optics and Photonics, (2018).

[35] Y. Tan, et al. "Transferable tight-binding model for strained group IV and III-Vmaterials and heterostructures," *Phys. Rev. B* 94, 045311 (2016).

[36] F. Capasso, "Physics of avalanche photodiodes," *Semicond. Semimetals 22*, 1–172 (1985).

[37] S. Kwok, Phys. *Semicond. Dev.*, (2006).

[38] http://www.ioffe.ru/SVA/NSM/Semicond/GaInAsSb/bandstr.html

[39] Y. Yuan, et al. "AlInAsSb Impact Ionization Coefficients," *IEEE Photo. Tech. Lett*. 31, 315-318 (2019).

[40] X. G. Zheng, et al. "Temperature dependence of the ionization coefficients of AlxGa1-xAs," *IEEE J. Quantum Electron.* 36, 1168–1173 (2000).